Materials Transactions, Vol. 60, No. 9 (2019) pp. 1755 to 1762
Special Issue on Latest Research and Development of Structural and Functional Titanium-Based Materials

Low Springback and Low Young's Modulus in Ti–29Nb–13Ta–4.6Zr Alloy Modified by Mo Addition

Qiang Li[1,*], Qiang Qi[1], Junjie Li[2], Masaaki Nakai[3], Mitsuo Niinomi[1,4,5,6,*], Yuichiro Koizumi[5], Daixiu Wei[4,*], Kenta Yamanaka[4], Takayoshi Nakano[5], Akihiko Chiba[4], Xuyan Liu[1] and Deng Pan[7]

[1]*School of Mechanical Engineering, University of Shanghai for Science and Technology, Shanghai 200093, P. R. China*
[2]*International Iberian Nanotechnology Laboratory, Av. Mestre José Veiga s/n, 4715-330 Braga, Portugal*
[3]*Department of Mechanical Engineering, Faculty of Science and Engineering, Kindai University, Higashiosaka 577-8502, Japan*
[4]*Institute for Materials Research, Tohoku University, Sendai 980-5377, Japan*
[5]*Department of Materials and Manufacturing Science, Graduate School of Engineering, Osaka University, Suita 565-0871, Japan*
[6]*Department of Materials Science and Engineering, Graduate School of Science and Technology, Meijo University, Nagoya 468-8502, Japan*
[7]*Materials Genome Institute, Shanghai University, Shanghai 200444, China*

Deformation-induced higher Young's modulus can satisfy the contradictory requirements of Ti alloys for spinal-fixation applications, which demand a high Young's modulus to reduce springback during operations and a low Young's modulus to prevent stress shielding effect for patients after surgeries. In this study, TNTZ–(1, 3, 5)Mo are designed by adding Mo and Ti to Ti–29Nb–13Ta–4.6Zr (TNTZ) in order to maintain low initial Young's modulus and achieve low springback. All the solutionized alloys show single β phase with increasing the β stability by Mo addition. They show low Young's moduli less than 65 GPa, similar ultimate tensile strength of 650 MPa and elongation around 20%. The springback of TNTZ–3Mo and TNTZ–5Mo is lower than that of TNTZ and TNTZ–1Mo owing to their more stable β phase. After cold rolling, TNTZ–3Mo shows the largest increasing ratio of 25% in Young's modulus and the highest ultimate tensile strength owning to the appearance of deformation-induced ω phase. With the low initial Young's modulus of 59 GPa, TNTZ–3Mo is a potential candidate to make the spinal rods in spinal fixation devices. [doi:10.2320/matertrans.ME201912]

(Received January 29, 2019; Accepted May 16, 2019; Published July 5, 2019)

Keywords: *biomaterial, titanium alloy, mechanical property, springback, deformation mechanism*

1. Introduction

The need for metallic bio-implant materials has risen sharply with the continual growth of the aged population and the increase in traffic accidents especially for young people, who need replacement surgeries for functionally failed hard tissue.[1,2] Currently, metallic bio-implant materials consist chiefly of SUS316L stainless steel, commercial pure titanium (CP Ti), and Ti–6Al–4V extra-low interstitial alloy (Ti64 ELI).[3–5] However, all these materials have found some shortcomings. SUS316L contains allergy element Ni[6,7] and affects magnetic resonance imaging (MRI) diagnosis for its ferromagnetism.[8] The mechanical properties of CP Ti are moderate. Ti64 ELI contains toxic element V and neurotoxic element Al.[9,10] In addition, the Young's Modulus of these biomaterials is much higher than that of human bone (10–30 GPa),[11] which will bring a stress shielding effect causing failure of implants.[12] Therefore, much effort has been devoted to developing novel Ti alloys containing nontoxic and nonallergic elements and having a low Young's modulus (40–60 GPa).[3,4,13,14] It has been reported that β-type Ti–29Nb–13Ta–4.6Zr (mass%, TNTZ) exhibits excellent mechanical properties, corrosion resistance and biocompatibility, and low Young's modulus.[13,15] It has been considered to be a potential candidate for use as a metallic implant biomaterial, and it has been applied to the production of rod implants for spinal fixation applications.

However, the implant rod with a low Young's modulus couldn't meet all the requirements of successful implantation surgeries for patients. The rods manipulated by a surgeon to follow the shape of the spine should also have low springback after implantation surgery.[16] The magnitude of springback is related to both the strength and the Young's modulus of the implant rod. If two rods have the same strength, the rod with a higher Young's modulus exhibits a lower springback. Therefore, the alloys for spinal fixation applications should have changeable Young's modulus to meet inconsistent requirements, which demand a low Young's modulus to prevent the stress shielding effect and a high Young's modulus to suppress springback during implantation surgeries.[17] It has been reported that some metastable β-type Ti alloys appear a non-equilibrium phase during deformation, such as α', α'', and ω.[18–21] In addition, the Young's modulus of the deformation-induced ω phase is often higher than that of the β phase.[22–24] Therefore, the deformation-induced ω phase makes it possible to increase the Young's modulus at certain parts of the rod by deformation, while the rest non-deformed part of the rod can remain its low Young's modulus.

It has been confirmed that metastable β-type Ti alloys can easily obtain deformation-induced ω transformation by adding Cr and Mo.[25] However, the initial Young's moduli of binary Ti–Cr and Ti–Mo alloys are higher than 65 GPa. The potential toxicity and allergenicity of Cr are still worrying.[26] In this study, Ti–29Nb–13Ta–4.6Zr with Mo addition were designed and investigated on their microstructure, deformation mechanism, mechanical properties, springback and change in Young's modulus due to deformation.

*Corresponding authors, E-mail: jxli@tju.edu.cn & liqiang@usst.edu.cn, niinomi@imr.tohoku.ac.jp, wei1987xiu@imr.tohoku.ac.jp

Table 1 Chemical compositions and Mo_{eq} of TNTZ and TNTZ–(1, 3, 5)Mo.

Alloy \ Chemical composition		Ti	Nb	Ta	Zr	Mo	Mo_{eq}
TNTZ	Nominally	Bal.	29	13	4.6	-	10.98
	Obtained	Bal.	28.15	12.75	4.56	-	10.69
TNTZ-1Mo	Nominally	Bal.	27.84	12.48	4.42	1	11.54
	Obtained	Bal.	27.60	12.80	4.34	1.02	11.56
TNTZ-3Mo	Nominally	Bal.	25.52	11.44	4.05	3	12.66
	Obtained	Bal.	25.15	10.80	4.05	3.13	12.55
TNTZ-5Mo	Nominally	Bal.	23.2	10.4	3.68	5	13.78
	Obtained	Bal.	22.8	10.40	3.59	5.09	13.76

2. Experiments

2.1 Alloy design

Mo shows better ability to stabilize the β phase than Nb and Ta. To avoid obtaining the excessive stable β phase, pure Ti and Mo with the mass ratio of 3:1, were added to TNTZ. 1%, 3%, and 5% of Mo in mass% were added by adjusting the ratio of Ti, Mo and TNTZ, respectively. Mo equivalents (Mo_{eq}) of Ti alloys are usually used to evaluate the stability of the β phase.[27] The designed composition, the analyzed composition, and the Mo_{eq} values of the alloys are listed in Table 1. The β phases in designed alloys become more stable with increasing Mo content owning to the raise of Mo_{eq}.

2.2 Material preparation

The ingots with the nominal compositions in Table 1 were prepared by non-consumable arc melting mixtures of pure Ti (99.999 mass%), Nb (99.95 mass%), Ta (99.95 mass%), Zr (99.95 mass%), and Mo (99.95 mass%) in a high purity argon atmosphere. The obtained ingots were homogenized at 1373 K for 21.6 ks in an argon atmosphere followed by water quenching. The ingots were then cold-rolled into plates with a total reduction ratio around 83% at room temperature without intermediate annealing. The cold-rolled plates were subjected to solution treatment (ST) at 1123 K for 3.6 ks in vacuum conditions followed by water quenching. For convenience, TNTZ, TNTZ–1Mo, TNTZ–3Mo, and TNTZ–5Mo after ST are referred to as TNTZ–ST, TNTZ–1Mo–ST, TNTZ–3Mo–ST, and TNTZ–5Mo–ST, respectively. Then, cold rolling (CR) was performed again on some solution-treated specimens with a reduction ratio of 10% at room temperature in order to evaluate the Young's modulus and tensile properties after deformation instead of bending. TNTZ, TNTZ–1Mo, TNTZ–3Mo, and TNTZ–5Mo after the final cold rolling are referred to as TNTZ–CR, TNTZ–1Mo–CR, TNTZ–3Mo–CR, and TNTZ–5Mo–CR, respectively.

2.3 Microstructural characterization

The phase constitutions were identified by X-ray diffraction (XRD) using a Bruker D8 X-ray diffractometer with Cu Kα radiation at a voltage of 40 kV and a current of 40 mA. The microstructures were observed by optical microscopy (OM) and electron backscattered diffraction (EBSD). For the observations, the specimens were mechanically ground using SiC waterproof papers up to 2400# grit and polished by a colloidal SiO_2 suspension. The mirror-polished specimens were then etched in a 5-vol% hydrofluoric acid (HF) solution for approximately 45 s. Specimens for transmission electron microscopy (TEM) observations were mechanically polished to a thickness of approximately 50 μm, dimpled by a phosphor bronze ring to approximately 15 μm, and then ion-milled to a thin foil. TEM measurements were performed using a JEOL JEM-2000EX TEM at a voltage of 200 kV.

2.4 Evaluation of mechanical properties and springback

The sizes of specimens for tensile tests, Young's modulus measurements and bending tests were 12 mm × 3 mm × 1.5 mm for the gage part, 40 mm × 10 mm × 1.5 mm, and 40 mm × 5 mm × 1.5 mm, respectively. The specimens were cut by wire electric discharge machining. Young's moduli were measured by free resonance method at ambient temperature. Tensile tests were carried out at a strain speed of $6.94 \times 10^{-4}\,s^{-1}$ using an Instron-type testing machine at room temperature, with a fixed strain gauge to improve the measurement accuracy.

Both tensile and bending loading–unloading tests were carried out at room temperature to evaluate the springback of the specimens after ST. For tensile loading–unloading tests, the strain was applied from 1 to 10% with a step of 1%. The ratio (R) of springback (recovery strain) per unit load to the applied strain was calculated based on the data obtained from the tensile loading–unloading curves, as described in previous studies.[17,20,21] The distance between the two parallel supports for the samples was 30 mm in bending tests. The indenter was driven down to the specimens at a speed of $8.33 \times 10^{-6}\,m{\cdot}s^{-1}$ until a deflection of 3.0 mm was achieved, and then it was raised up at the same speed until the force was reduced to 0 N.

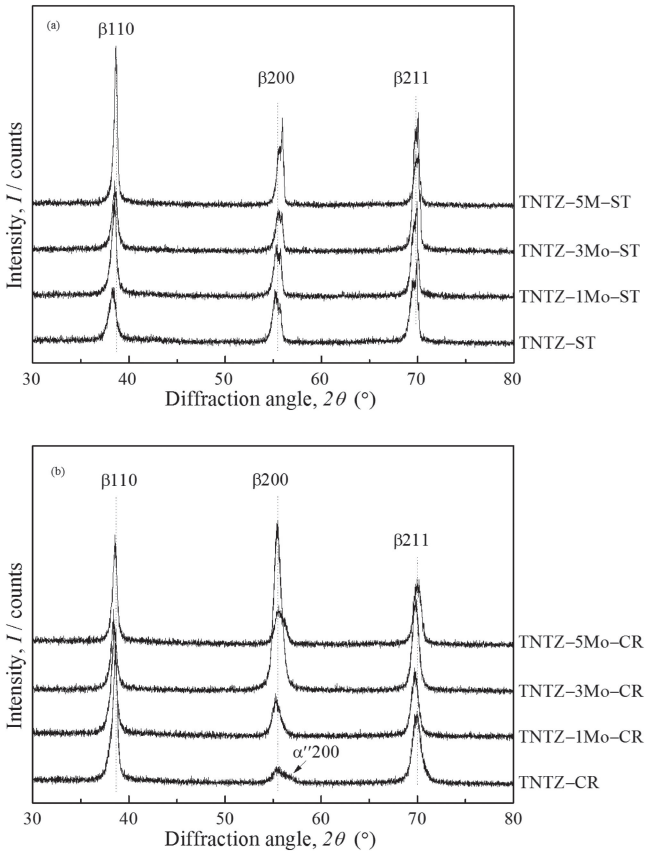

Fig. 1 XRD patterns of TNTZ and TNTZ–(1, 3, 5)Mo subjected to (a) solution treatment (ST) and (b) cold rolling (CR).

3. Results and Discussion

3.1 Microstructures

Figure 1 shows the XRD profiles of TNTZ, TNTZ–1Mo, TNTZ–3Mo, and TNTZ–5Mo after ST and CR. All the solution-treated alloys show only the peaks of the β phase in the XRD patterns (Fig. 1(a)). After CR, some weak peaks corresponding to the α'' phase appear in TNTZ–CR (Fig. 1(b)), which indicates that deformation-induced α'' martensite occurs in TNTZ during CR. No new peaks are present in TNTZ–1Mo–CR, TNTZ–3Mo–CR, and TNTZ–5Mo–CR.

All the solutionized TNTZ and TNTZ–(1, 3, 5)Mo samples consist of equiaxed β grains with sizes of 20∼50 μm without any precipitates (Figs. 2(a)–(d)). Difference is hardly found in optical microstructure of the four alloys with different Mo content. Mo doesn't lead to the grain refinement or grain coarsening.

After CR, a few deformation bands are observed in the equiaxed grains in TNTZ–CR, TNTZ–1Mo–CR, and TNTZ–3Mo–CR (Fig. 3(a)–(c)). However, no change could be observed in TNTZ–5Mo–CR (Fig. 3(d)) comparing with TNTZ–5Mo–ST (Fig. 2(d)). The bands in TNTZ–CR are defined as $\{332\}_\beta\langle 113\rangle_\beta$ twining owing to TEM and EBSD results in previous research.[15] In this study, EBSD also show clear bands in the inverse pole figures (IPFs) of TNTZ–1Mo–CR and TNTZ–3Mo–CR, as shown in Figs. 4(a) and 4(d), respectively. The boundaries with rotation angle of 48°∼53° are marked as blue lines in the grain boundary map (Fig. 4(b)). The crystal misorientation between the matrix and the band is near 50.5° in TNTZ–1Mo–CR, as indicated by the blue lines in Fig. 4(b) and shows in Fig. 4(c). The bands can be delineated as $\{332\}_\beta\langle 113\rangle_\beta$ twining because the misorientation between matrix and $\{332\}_\beta\langle 113\rangle_\beta$ twining along the $\langle 110\rangle_\beta$ direction is 50.5°.[28,29] However, no blue line is marked in the grain boundary map of TNTZ–3Mo–CR (Fig. 4(e)). The misorientation between the band and the matrix in TNTZ–3Mo–CR is just 14° to 26° (Fig. 4(f)), which is different from twining. Therefore, $\{332\}_\beta\langle 113\rangle_\beta$

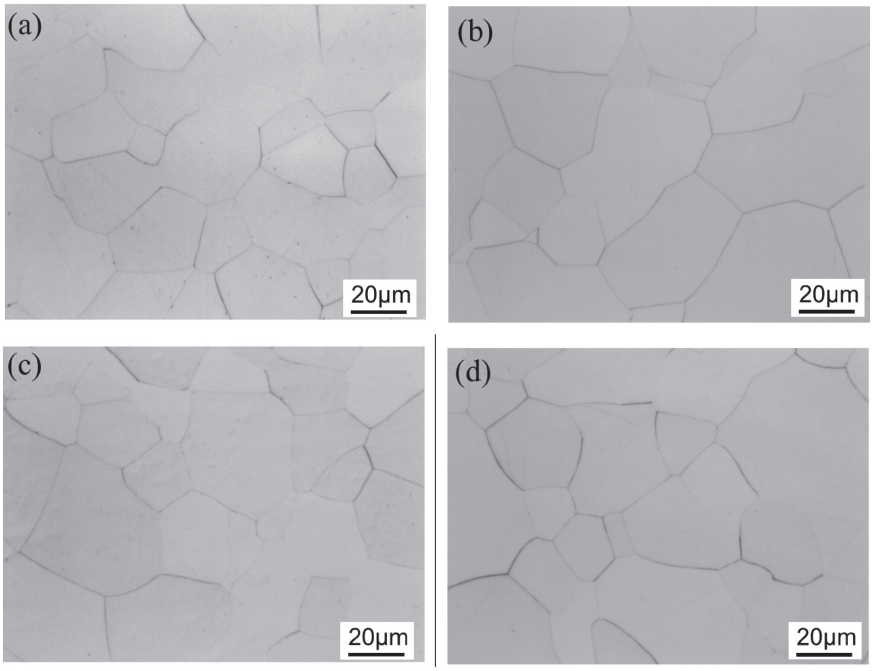

Fig. 2 Optical micrographs of TNTZ and TNTZ–(1, 3, 5)Mo subjected to solution treatment (ST): (a) TNTZ–ST, (b) TNTZ–1Mo–ST, (c) TNTZ–3Mo–ST and (d) TNTZ–5Mo–ST.

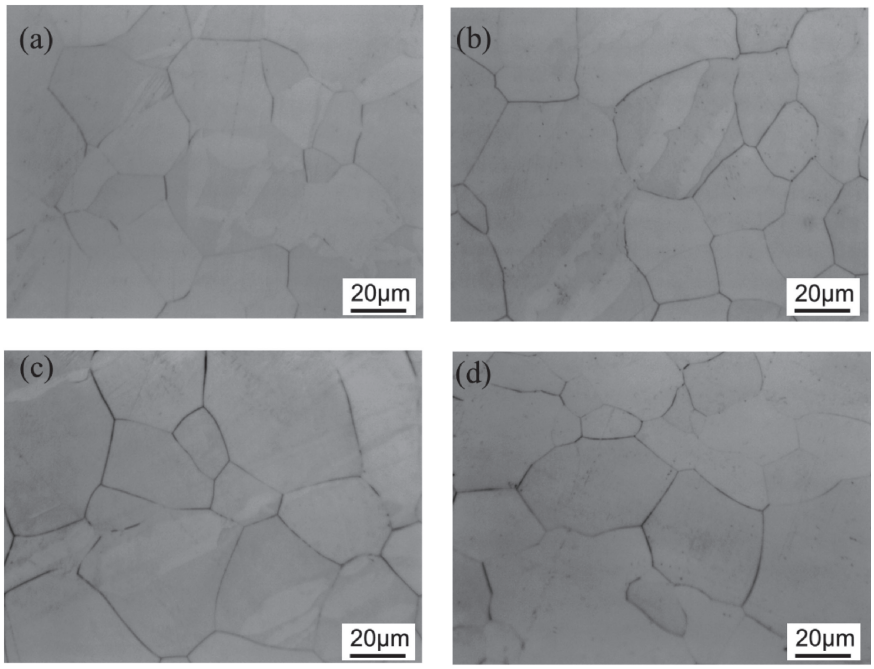

Fig. 3 Optical micrographs of TNTZ and TNTZ–(1, 3, 5)Mo subjected to cold rolling (CR): (a) TNTZ–CR, (b) TNTZ–1Mo–CR, (c) TNTZ–3Mo–CR and (d) TNTZ–5Mo–CR.

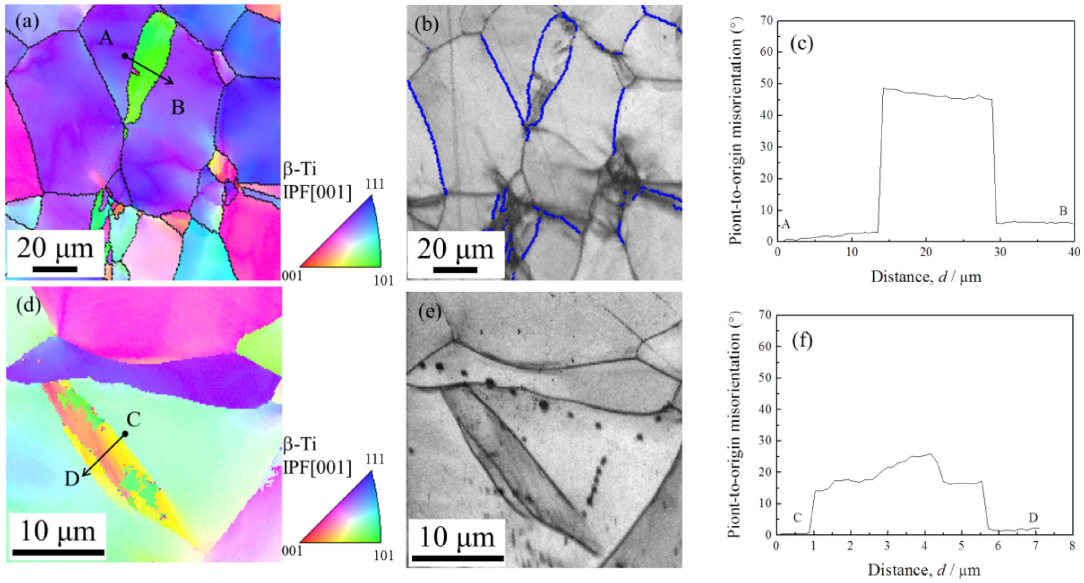

Fig. 4 EBSD maps of (a)~(c) TNTZ–1Mo–CR, and (d)~(f) TNTZ–3Mo–CR: (a) and (d) IPF figures, (b) and (e) grain boundary map, and (c) and (f) misorientations relative to the first point along the arrow in (a) and (d), respectively.

twining exists in TNTZ–CR and TNTZ–1Mo–CR but disappears in TNTZ–3Mo–CR and TNTZ–5Mo–CR with further increased β stability.

There is single β phase in TNTZ–3Mo–ST based on the TEM bright field image and selected area electron diffraction (SAED) pattern, as shown in Figs. 5(a) and 5(b). Besides diffraction spots of β phase, some weak diffraction spots are also observed in the SAED pattern of TNTZ–3Mo–CR. The spots are similar to those of the cold rolled Ti–12Cr alloy, which shows deformation induced ω phase transformation.[17] The TEM results indicate that deformation induced ω phase transformation occurs in TNTZ–3Mo during cold rolling. TNTZ–CR, TNTZ–1Mo–CR, and TNTZ–5Mo–CR show only diffraction patterns of single β phase. For TNTZ and TNTZ–1Mo, deformation-induced α'' martensite transformation and $\{332\}_\beta\langle113\rangle_\beta$ twining are the main deformation mechanism owning to the metastable β phase. TNTZ–5Mo has ultra-stable β phase, thus twining and deformation-induced phase transformation hardly occur.

3.2 Mechanical properties

3.2.1 Young's modulus

Figure 6 shows the comparisons in Young's modulus of the four alloys subjected to ST and CR. As pointed above, the solutionized alloys consist of a single β phase. Therefore, they all exhibit low Young's moduli of <65 GPa. TNTZ–ST

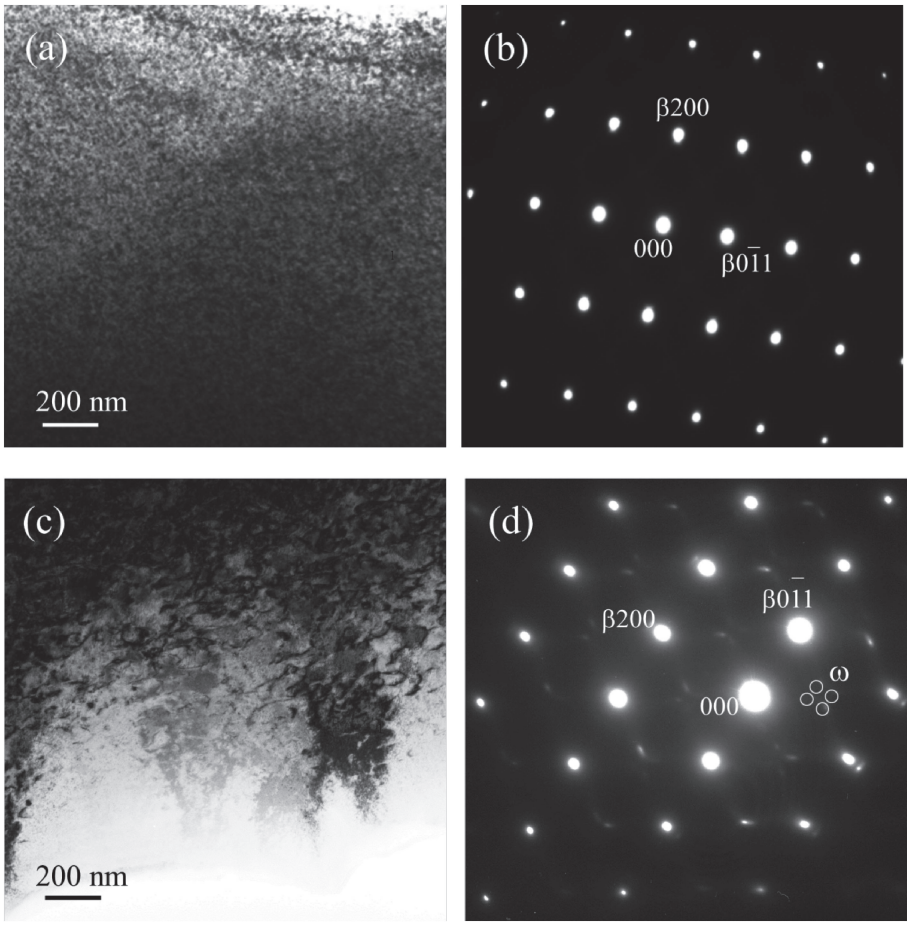

Fig. 5 TEM images obtained from TNTZ–3Mo: (a) bright-field image and (b) diffraction pattern subjected to solution treatment (ST); (c) bright-field image and (d) diffraction pattern subjected to cold rolling (CR). The beam direction is parallel to $[011]_{\beta}$.

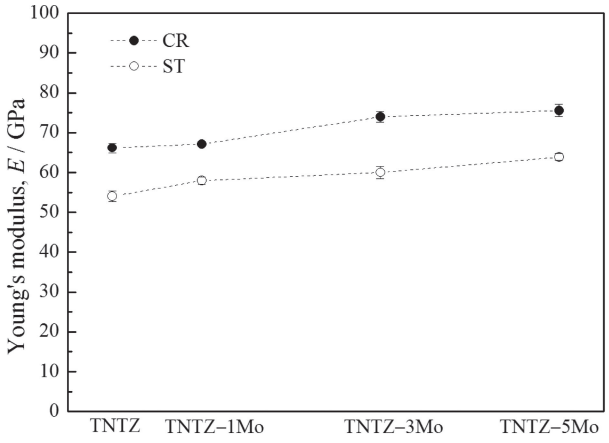

Fig. 6 Young's modulus of TNTZ and TNTZ–(1, 3, 5)Mo subjected to solution treatment (ST) and cold rolling (CR).

shows the lowest Young's modulus around 55 GPa. The Young's modulus is slightly increased with increasing Mo content. The Young's moduli of TNTZ–1Mo–ST, TNTZ–3Mo–ST, and TNTZ–5Mo–ST are around 58 GPa, 59 GPa, and 64 GPa, respectively. The Young's moduli of solution-ized specimens in present study are lower than SUS316L, CP Ti, and Ti64 ELI,[3,5] and also lower than some other β-type Ti alloys with changeable Young's modulus, such as Ti–(15∼18)Mo and Ti–(10∼14)Cr.[20,21]

The Young's moduli of the four alloys increase after CR. There are two main factors influencing the Young's modulus of the cold rolled specimens in this study. The one is the appearance of deformation-induced phase transformation, because the Young's modulus is determined by the moduli of the individual phases and their volume fraction.[30,31] The other one is the lattice distortion. The process of CR decreases the atomic distance, increases the defects, internal stress and bond strength of atom, and finically causes an increment in Young's modulus. Although deformation-induced α'' phase with a lower Young's modulus appears in TNTZ–CR, the latter factor shows greater effect than the former one. Therefore, TNTZ exhibits higher Young's modulus after CR. There is no deformation-induced α'' phase in TNTZ–(1, 3, 5)Mo–CR. Thus, the Mo modified TNTZ all shows obvious increase in Young's moduli after CR. Furthermore, deformation-induced ω phase with a higher Young's modulus is found in TNTZ–3Mo–CR. It shows a Young's modulus up to 74 GPa, which is increased by 25% comparing with TNTZ–3Mo–ST. The increase ratio (∼25%) of Young's modulus for TNTZ–3Mo is similar as that of Ti–11Cr (∼25%, from 68 to 85 GPa), and much higher than that of Ti–12Mo (∼15%, from 73 to 84 GPa).

3.2.2 Tensile properties

Figure 7 shows the tensile stress–strain curve of the four alloys subjected to ST and subsequently CR, respectively. TNTZ–ST shows a non-linear deformation behavior between

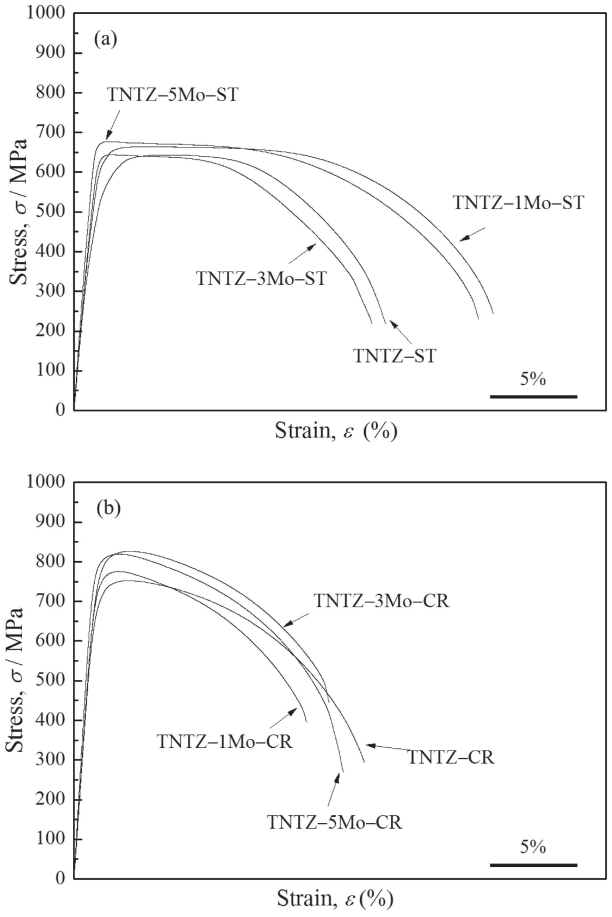

Fig. 7 Stress–strain curves obtained from tensile tests of TNTZ and TNTZ–(1, 3, 5)Mo subjected to (a) solution treatment (ST) and (b) cold rolling (CR).

elastic deformation and plastic deformation rather than obvious yielding. The non-linear deformation behavior is suppressed with the increase of β stability. Obvious yielding can be seen in TNTZ–5Mo–ST because the β phase is stable. Although twins have been pointed out to cause an increase of strength in some other β-type Ti alloys during tension,[32] work-hardening rarely appears in TNTZ–ST and TNTZ–1Mo–ST because there are only small amount of twins locally appearing in the β grain. The non-linear deformation behavior almost disappears after CR.

Figure 8 shows the tensile properties obtained by tensile tests. With the increase of β stability, the 0.2% proof stress is raised owning to the gradually demission of non-linear deformation behavior in the solutionized specimens. Mo is supposed to bring solution hardening, but the decreasing amount of other alloying elements reduces the hardening effect. Therefore, TNTZ–ST and TNTZ–(1, 3, 5)Mo–ST show near the same ultimate tensile strength of 650 MPa. The elongations are all higher than 20%, which is acceptable for biomedical application. Cold rolling always causes internal stress and defects in the alloys and then brings hardening effect. Both the 0.2% proof stress and tensile strength are significantly increased after cold rolling. It's noticed that the 0.2% proof stress and tensile strength are increased with Mo addition firstly and reach the highest value in TNTZ–3Mo–CR. TNTZ–5Mo–CR shows lower tensile strength and similar 0.2% proof stress comparing with TNTZ–3Mo–CR.

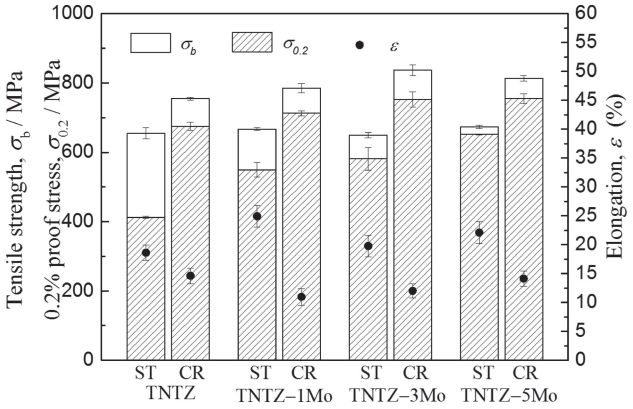

Fig. 8 Tensile properties of TNTZ and TNTZ–(1, 3, 5)Mo subjected to solution treatment (ST) and cold rolling (CR).

According to TEM results, the ω phase appears in TNTZ–3Mo–CR. Therefore, the increase in the 0.2% proof stress and tensile strength of TNTZ–3Mo–CR is considered to be derived from the deformation-induced ω phase transformation. Although the elongation is decreased by CR, all the cold rolled specimens show elongation around 15%, indicating good plasticity.

3.3 Springback

3.3.1 Tensile loading–unloading characteristics

The R value is calculated from the tensile loading–unloading for comparing the springback of the alloys as shown in Fig. 9. All the alloys show similar trend of R values as a function of the applied tensile strain. As the applied tensile strain increases from 1% to 4%, the first decrease in R values is owing to the increase in stress during tension. It can be seen from the stress–strain curves (Fig. 7) that the stress increases before the stress plateau. The stress plateaus in TNTZ–ST, TNTZ–1Mo–ST, TNTZ–3Mo–ST, and TNTZ–5Mo–ST begin at the strains of 3.9%, 3.2%, 2.2% and 1.8%, respectively. When the stress is constant under higher strain level, the recovery becomes constant and makes R value stable. The critical strains for stable R values of TNTZ–ST, TNTZ–1Mo–ST, TNTZ–3Mo–ST, and TNTZ–5Mo–ST are

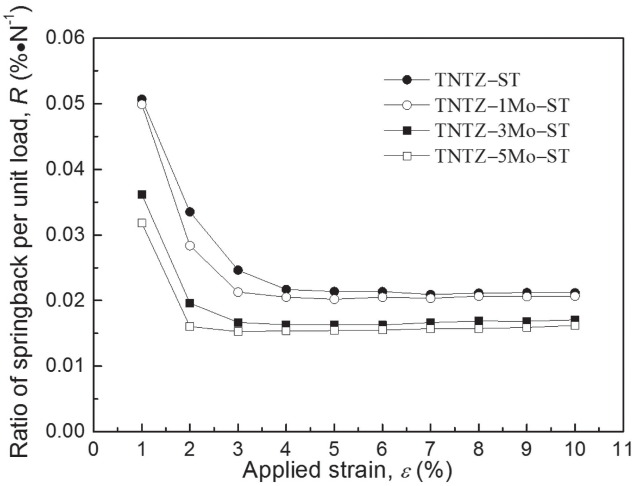

Fig. 9 Ratio of springback per unit load (R) as a function of applied strain for TNTZ and TNTZ–(1, 3, 5)Mo subjected to solution treatment (ST).

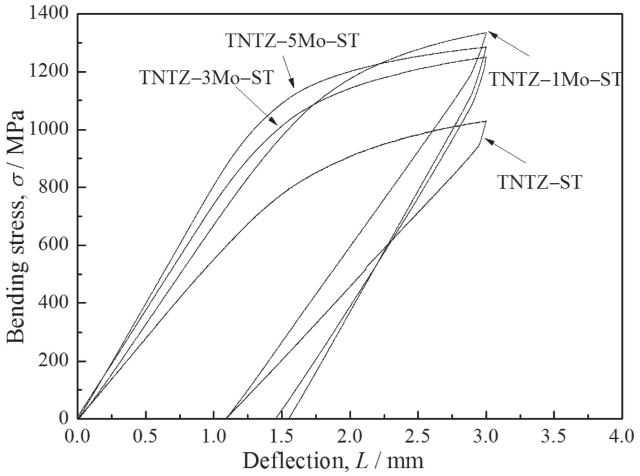

Fig. 10 Stress–deflection curves obtained from bending loading–unloading tests of TNTZ and TNTZ–(1, 3, 5)Mo subjected to solution treatment (ST).

4.0%, 4.0%, 3%, and 2%, respectively, which are just above the strains corresponding to the starting of stress plateaus. TNTZ–ST and TNTZ–1Mo–ST show the similar R values at higher applied strain indicating that they own similar springback. TNTZ–3Mo–ST and TNTZ–5Mo–ST also show nearly the same and lower R values, thus they have lower springback than TNTZ–ST and TNTZ–1Mo–ST. The R values of TNTZ–3Mo–ST and TNTZ–5Mo–ST are also lower than those of Ti–17Mo and Ti–30Zr–3Cr–3Mo, which have been designed to obtain low springback.[20,25] Thus, TNTZ–3Mo and TNTZ–5Mo are more easily deformed to certain shapes for surgeons during surgeries.

3.3.2 Bending loading–unloading characteristics

Materials for spinal-fixation applications are usually bended to follow the curvature of the spine by surgeon during surgery. It's believed that three-point bending is one of the most intuitive methods to simulate the bending process during surgery. Figure 10 shows the stress–deflection curves obtained by three-point bending loading–unloading tests of TNTZ–ST and TNTZ–(1, 3, 5)Mo–ST. TNTZ–1Mo–ST exhibits the same springback with TNTZ–ST. Both the residual deflection values are ∼1.10 mm after unloading from a deflection of 3.00 mm to a stress of zero, thus a recovery deflection value of ∼1.90 mm is obtained in both TNTZ–ST and TNTZ–1Mo–ST. However, the recovery deflection values of TNTZ–3Mo–ST and TNTZ–5Mo–ST were only ∼1.55 mm and ∼1.45 mm, respectively, which are much lower than TNTZ–ST and TNTZ–1Mo–ST. The bending loading–unloading results are quite consisted with the calculation of R values, which indicates that TNTZ–3Mo and TNTZ–5Mo show lower springback.

3.4 Discussion

In this study, solutionized TNTZ and TNTZ–(1, 3, 5)Mo all show similar mechanical properties and deformation-induced higher Young's modulus. Low Young's modulus is always obtained in the Ti alloys with meta-stable β phase. The addition of Mo slightly increases the β stability. Therefore, the Young's modulus shows the lowest value in TNTZ with meta-stable β phase and is slightly increased with increasing β stability. The similar strength and elongation are also due to the similar strengthening effect by alloying elements.

However, their springback values are different. The main reason for these phenomena is the different deformation mechanism determined by β stability. As mentioned above, lattice distortion is the dominant fact and causes the increase of Young's modulus. TNTZ and TNTZ–(1, 3, 5)Mo all show deformation-induced higher Young's modulus. Springback is determined by the recovery, which originates from elastic recovery of β phase and pseudo-elastic recovery in meta-stable β phase. Pseudo-elastic recovery dominates the springback of meta-stable β-type Ti alloys, although higher Young's modulus causes lower elastic recovery. According to the tensile stress–strain curves and microstructures, nonlinear deformation behavior and deformation-induced α'' martensite are observed in TNTZ. The large springback owns to the meta-stable β phase. Deformation-induced α'' is suppressed in TNTZ–1Mo, but the existence of nonlinear deformation behavior indicates a meta-stable β phase. Thus, TNTZ–1Mo also shows large springback. TNTZ–3Mo and TNTZ–5Mo show lower springback owing to the more stable β phase. The absence of nonlinear deformation and existence of deformation-induced higher Young's modulus both can reduce recovery and decrease springback.

Although it's a contradictory to obtain both low initial Young's modulus and low springback in Ti alloys with meta-stable or stable β phase, it can be solved by appropriate adjusting the β stability. It's well known that Mo shows lower ability to stabilize β phase comparing with Cr, which has been used to modify TNTZ in our previous study.[15] The β stability of TNTZ is more carefully adjusted by Mo in this study. TNTZ–3Mo with suitable β stability shows the lowest initial Young's modulus (∼59 GPa) among alloys designed for the deformation-induced higher Young's modulus, including Ti–Cr, Ti–Mo, TNTZ–Cr, and Ti–30Zr–Cr–Mo alloys. It also shows highest strength after CR among TNTZ and TNTZ–(1, 3, 5)Mo owning to the deformation-induced ω phase. Thus, the shape of TNTZ–3Mo is difficult to change after deformation. In the other words, TNTZ–3Mo can preserve the fixed shape after operation, which is advantageous to spinal-fixation applications.

4. Conclusions

1%, 3%, and 5% of Mo in mass% are added together with pure Ti to Ti–29Nb–13Ta–4.6Zr in order to achieve low springback. The following conclusions can be drawn on the basis of obtained results in this study:

(1) The β phase stability in TNTZ and TNTZ–(1, 3, 5)Mo is gradually increased by Mo addition. After cold rolling, deformation-induced α'' phase and twins are observed in TNTZ. The twins are also found in TNTZ–1Mo, but disappear in TNTZ–(3, 5)Mo.

(2) The solutionized TNTZ and TNTZ–(1, 3, 5)Mo show similar ultimate tensile strength around 650 MPa. The 0.2% proof stress is raised with increasing Mo content, because non-linear tensile behavior is gradually suppressed. Young's modulus is slightly increased by Mo addition, but the maxim value is just 64 GPa in TNTZ–5Mo.

(3) Ultimate tensile strength, 0.2% proof strength and Young's moduli are increased by cold rolling in all the studied alloys. TNTZ–3Mo shows the highest strength and increasing ratio of Young's modulus owing to the deformation-induced ω transformation.
(4) TNTZ–3Mo and TNTZ–5Mo show less springback than the original TNTZ due to their a little more stable β phase. Particularly, TNTZ–3Mo with a low initial Young's modulus of 59 GPa is advantageous for spinal-fixation applications.

Acknowledgement

This work was partially supported by the Natural Science Foundation of Shanghai, China (No. 15ZR1428400), Shanghai Key Technology Support Program (No. 16060502400), National Natural Science Foundation of China (No. 61504080), the project of Creation of Life Innovation Materials for Interdisciplinary and International Researcher Development, Tohoku University, Japan sponsored by Ministry, Education, Culture, Sports, Science and Technology, Japan, and the Grant-in Aid for Scientific Research (B) (No. 17H03419) from Japan Society for the Promotion of Science (JSPS), Tokyo, Japan.

REFERENCES

1) M. Niinomi: Metall. Mater. Trans. A **33** (2002) 477–486.
2) M. Abdel-Hady and M. Niinomi: J. Mech. Behav. Biomed. Mater. **20** (2013) 407–415.
3) S. Mukhtar, W. Asghar, Z. Butt, Z. Abbas, M. Ullah and R. Atta-Ur-Rehman: J. Cent. South Univ. **25** (2018) 2578–2588.
4) M. Niinomi, M. Nakai and J. Heida: Acta Biomater. **8** (2012) 3888–3903.
5) M. Niinomi: Mater. Trans. **59** (2018) 1–13.
6) M. Mikulewicz and K. Chojnacka: Biol. Trace Elem. Res. **142** (2011) 865–889.
7) J. Sevcikova and M.P. Goldbergova: Biometals **30** (2017) 163–169.
8) T. Hanawa: J. Artif. Organs **12** (2009) 73–79.
9) J. Domingo: Biol. Trace Elem. Res. **88** (2002) 97–112.
10) M. Fellah, L. Aissani, M.A. Samad, A. Iost, T.M. Zine, A. Montagne and C. Nouveau: Acta Metall. Sin. (Engl. Lett.) **30** (2017) 1089–1099.
11) J.Y. Rho, T.Y. Tsui and G.M. Pharr: Biomaterials **18** (1997) 1325–1330.
12) N. Sumitomo, K. Noritake, T. Hattori, K. Morikawa, S. Niwa, K. Sato and M. Niinomi: J. Mater. Sci. **19** (2008) 1581–1586.
13) M. Morinaga: Mater. Trans. **57** (2016) 213–226.
14) T. Morita, N. Uehigashi and C. Kagaya: Mater. Trans. **54** (2013) 22–27.
15) Q. Li, M. Niinomi, J. Hieda, M. Nakai and K. Cho: Acta Biomater. **9** (2013) 8027–8035.
16) J.P. Steib, R. Dumas, D. Mitton and W. Skall: Spine. **29** (2004) 193–199.
17) M. Nakai, M. Niinomi, X.F. Zhao and X.L. Zhao: Mater. Lett. **65** (2011) 688–690.
18) R.M. Wood: Mater. Lett. **65** (2011) 688–690.
19) Y. Shinohara, M. Tahara, T. Inamura, S. Miyazaki and H. Hosoda: Mater. Trans. **56** (2015) 404–409.
20) X.F. Zhao, M. Niinomi, M. Nakai and J. Hieda: Acta Biomater. **8** (2012) 1990–1997.
21) X.F. Zhao, M. Niinomi, M. Nakai, J. Hieda, T. Ishimoto and T. Nakano: Acta Biomater. **8** (2012) 2392–2400.
22) Q. Li, J.J. Li, G.H. Ma, X.Y. Liu and D. Pan: Mater. Des. **111** (2016) 421–428.
23) H.H. Liu, M. Niinomi, M. Nakai, K. Cho and H. Fujii: Scr. Mater. **130** (2017) 27–31.
24) Y.L. Hao, R. Yang, M. Niinomi, D. Kuroda, Y.L. Zhou, K. Fukunaga and A. Suzuki: Metall. Mater. Trans. A **34** (2003) 1007–1012.
25) X.L. Zhao, M. Niinomi, M. Nakai, G. Miyamoto and T. Furuhara: Acta Biomater. **7** (2011) 3230–3236.
26) A.K. Shanker, C. Cervantes, L.T. Herminia and S. Avudainayagam: Environ. Int. **31** (2005) 739–753.
27) T. Zhou, M. Aindow, S.P. Alpay, M.J. Blackburn and M.H. Wu: Scr. Mater. **50** (2004) 343–348.
28) E. Bertrand, P. Castany, I. Péron and T. Gloriant: Scr. Mater. **64** (2011) 1110–1113.
29) M.J. Lai, C.C. Tasan and D. Raabe: Acta Mater. **111** (2016) 173–186.
30) S. Hanada, N. Masahashi and T.K. Jung: Mater. Sci. Eng. A **588** (2013) 403–410.
31) S. Gorsse, Y. Le Petitcorps, S. Matar and F. Rebillat: Mater. Sci. Eng. A **340** (2003) 80–87.
32) M. Marteleur, F. Sun, T. Gloriant, P. Vermaut, P.J. Jacques and F. Prima: Scr. Mater. **66** (2012) 749–752.